frontiers | Frontiers in Earth Science

ORIGINAL RESEARCH
published: 31 May 2022
doi: 10.3389/feart.2022.934452

Genesis Analysis of Ground Collapse in Wuhan Based on 3D Geological Model

Qi He[1], *Fei Tan*[1]*, *Zhaoliang Peng*[1], *Liang Tao*[2], *Yuyong Jiao*[1], *Shunchang Liu*[2] and *Hanfa Peng*[2]

[1]Faculty of Engineering, China University of Geosciences, Wuhan, China, [2]Wuhan Geomatic Institute, Wuhan, China

Ground collapse has been one of the main types of geological disasters in Wuhan City. It can be characterized by complex disaster-inducing environment, diverse disaster-causing factors, fragile disaster-bearing bodies, and serious consequences. In this study, a 3D geological structure model of the area was established by collecting data from major ground collapse incidents in Wuhan that have occurred over the years and by combining them with geological data obtained from boreholes. The model was used to analyze the distribution of ground subsidence in the city and reveal the geological causes of ground subsidence accidents in this area. The results showed that ground collapse is mainly distributed in the karst development area along the Yangtze River in Baishazhou. The karst was most developed at the intersection between the Yangtze River fault and the Hanyang fold belt. The ground collapse incidents showed two main characteristics in terms of their spatial distribution. Most of the collapse areas developed in the central third limestone belt. Most of the collapses are located on the first terrace of the Yangtze River. Most collapse points were controlled by geomorphic units (first terrace), stratigraphic age (Holocene) and stratigraphic combination (a binary structure composed of clay as the upper part and fine sand as the lower part, and the bottom is a gravel layer, containing pore confined water). The karst collapse in Fenghuo Village was selected as a case study to analyze the evolution process and disaster-causing mechanism of the karst collapse. Groundwater extraction was found to be the main reason for the karst collapse. The research results provide a geological basis for the planning layout and urban construction in Wuhan City.

Keywords: 3D geological model, ground collapse, distribution regularity, disaster mechanism, Wuhan city, karst

OPEN ACCESS

Edited by:
Xiaodong Fu,
Institute of Rock and Soil Mechanics (CAS), China

Reviewed by:
Chenxi Miao,
Taiyuan University of Technology, China
Qiao Wang,
Wuhan University, China

***Correspondence:**
Fei Tan
tanfei@cug.edu.cn

Specialty section:
This article was submitted to Geohazards and Georisks, a section of the journal Frontiers in Earth Science

Received: *02 May 2022*
Accepted: *18 May 2022*
Published: *31 May 2022*

Citation:
He Q, Tan F, Peng Z, Tao L, Jiao Y, Liu S and Peng H (2022) Genesis Analysis of Ground Collapse in Wuhan Based on 3D Geological Model. Front. Earth Sci. 10:934452. doi: 10.3389/feart.2022.934452

INTRODUCTION

In China, soluble rock covers an area of approximately 346.3×10^4 km^2, accounting for more than 1/3 of the land area. China is one of 16 countries with serious karst ground collapse problems. More than 30 large- and medium-sized cities and more than 420 counties and cities are in the high-risk areas of karst ground subsidence. More than 40 mines, 25 railway lines, and hundreds of reservoirs have suffered from karst ground collapse for a long time. Karst is most developed in Guangxi, Guizhou, Hunan, Jiangxi, Hubei and other provinces (regions). With economic development and urbanization, particularly with the continuous expansion of the scale of urban infrastructure construction, karst-inducing geology and geological disasters are becoming increasingly prominent in cities with a carbonate distribution (such as Guangzhou, Wuhan, and Guilin, etc.). Due to the characteristics of karst development, many karst voids (such as karst fissures, karst caves,

etc.) are often formed under the cover of Quaternary strata; these are close to the surface and closely related to human production activities. Human activities, such as excessive exploitation of karst water, surface water storage, and geotechnical engineering construction, may destabilize the karst voids and cause ground collapse accidents. Therefore, karst ground collapse disasters often occur in densely populated cities or traffic lines, threatening people's lives and property.

Karst ground collapse is the result of the joint destruction of the overlying soil and underlying soluble rock, which is significantly affected by the lithology and structure of the strata. Research on karst ground subsidence first appeared in Russian newspapers during the period 1771–1809. In 1914, Su Pan reported the issue of environmental changes induced by karst collapse. In 1973, Germany held the first International Symposium on "Karst Subsidence and Subsidence—Engineering Geological Issues Related to Soluble Rock" in Hannover. In 1978, the Western Kenta University established the Karst and Cave Research Center. Atzori et al. (2015) applied the InSAR technology to model the land subsidence along the Dead Sea coastline to study the spatiotemporal relationship between the degree of coastline land subsidence and karst collapse. This technique has been extended to other environments prone to collapse such as chemical sedimentary environments (Klimchouk and Andrejchuk, 2005; Yilmaz et al., 2011) and carbonate environments (Gutiérrez et al., 2014). Zuo et al. (2009) used the 3D seismic technology to detect the spatial form of Xieqiao karst collapse, and the DDA method to calculate the deformation field; the authors analyzed the collapse mechanism, and for the first time, studied the influence of rock friction angle on the collapse based on the DDA. Li et al. (2013) believed that the main factors affecting karst collapse include the degree of karst development, coverage conditions and hydrogeological conditions. Using the BP neural network theory, a disaster risk assessment model for Wuhan was established, and the karst collapse risk division was evaluated. Koutepov et al. (2008) found that when the force of gravity is greater than the soil strength, a change in the groundwater level in the carbonate aquifer will lead to ground collapse; the authors applied the GIS technology to delineate the potential gravity collapse and erosion of collapsed areas. He et al. (2004) believed that the water pressure effect was the main factor inducing karst collapse. Shalev and Lyakhovsky (2012) used a 2D elastic-plastic damage rheological numerical model based on collapse data to study the rheological properties of large-scale soil cover. Luo (2014) studied the distribution characteristics of karst collapse in Wuhan, the history of karst development, and the causes and mechanism of karst ground collapse. Feng et al. (2001) collected data from 654 karst collapse incidents that occurred in Guilin in the past 40 years and analyzed their genetic types and temporal and spatial distribution characteristics.

A visual 3D geological model can effectively reflect the strata distribution and structural planes in 3D space and help directly observe and analyze the relationship between engineering structures and unfavorable geological conditions such as fault zones and weak interlayers. Zhu et al. (2013) established a 3D geological model based on geological concepts to thoroughly understand the subsurface. In Paris, Gypsum dissolution can be the cause of damage associated with subsidence and collapse, Thierry et al. (2009) developed a multi-layer 3D geological model using the same 20 m mesh grid, integrating 21 lithostratigraphic units. The hazard prone areas were calculated by geostatistical methods from the archived descriptions of more than 3900 boreholes and from existing geological maps. In terms of construction and application of 3D geological models, it has been widely used in geological surveys (Kessler et al., 2009), geophysical inversion (He et al., 2014), 3D mine simulation (Vollgger et al., 2015), and water resource assessment (Hassen et al., 2016).

Research on karst ground collapse is relatively abundant. However, the visualization and analysis of karst ground collapse by means of 3D geological modeling is not yet mature. Based on previous research, this study considered the karst ground subsidence in Wuhan as the research object and two banks of the Yangtze River in the Baishazhou karst belt in the central and southern parts of the city as key research areas. The 3D geological modeling software was used to transform geological information with an uneven, discontinuous and scattered spatial distribution into a visual, continuous, and intuitive 3D geological body and 3D model of the karst distribution. It can reflect the actual underground geological karst. Combined with the 3D geological model and existing geological data, the temporal and spatial distributions of karst ground collapse in the study area and the geological reasons for the frequent occurrence of karst ground collapse accidents in this area were analyzed. The karst collapse area in Fenghuo Village was selected as a typical case, for which a 3D karst distribution model was established, and the evolution process and disaster mechanism of the collapse were analyzed.

BASIC SITUATION OF GROUND COLLAPSE IN WUHAN

The necessary and sufficient conditions for karst ground collapse are: 1) The bedrock is soluble carbonate rock, and the shallow karst caves are developed; 2) The overlying Quaternary loose deposits are generally not thick; 3) The dynamic condition of groundwater changes easily, and the velocity and hydraulic gradient of the groundwater near the interface between the bedrock and the soil layer produce a high hydrodynamic pressure, which has potential erosion ability, and soil particles are carried away by the water. Therefore, karst ground subsidence is generally distributed in areas with strong karst development and thin Quaternary loose cover and on both sides of the riverbed along the river.

Wuhan is located in the eastern Jianghan Plain, with a carbonate rock distribution area of approximately 1100 km^2, accounting for approximately 13% of the city's land area. Tectonically, it is located in two I-level tectonic units, the Qinling fold system and the Yangtze paraplatform. The terrain is low in the middle and flat in the south. It is surrounded by hills and ridges, and there are many low mountains in the north. The Indosinian movement at the end of Middle Triassic created the basic structural outline of Wuhan area and controlled the plane distribution of the carbonate strata. From north to south, six karst belts were formed: Tianxingzhou belt (L1), Bridge belt (L2), Baishazhou belt (L3), Zhuankou belt (L4), Junshan belt (L5), and Hannan belt (L6). **Figure 1** shows the distribution of the karst belts.

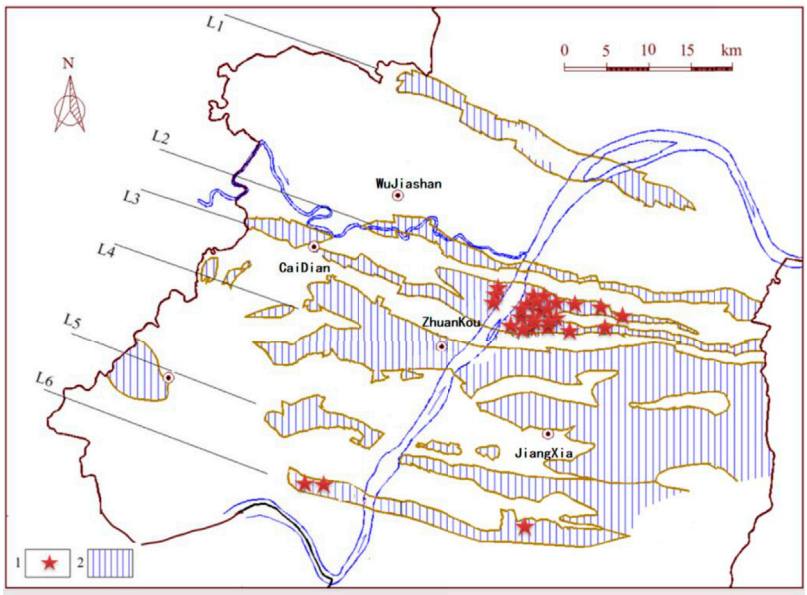

FIGURE 1 | Distribution diagram of karst belt and ground collapse in Wuhan City. 1. Karst ground collapse; 2. Karst belt.

The human engineering activities in Wuhan have destroyed the original geological environment conditions, leading to poor geological environment conditions, triggering and aggravating the occurrence of geological disasters. As of 13 January 2020, Wuhan has seen 125 existing geological disasters, including 32 ground collapses. The development scale of ground collapse in Wuhan is small. Currently, there are 31 small ground collapses and 1 medium ground collapse, accounting for 96.88 % and 3.12%, respectively. The medium-sized collapse is the ground collapse of Fenghuo Village. There are 22 collapse pits, with a total area of about 10400 m^2 and an average depth of 40 m. In small collapses, the distribution area of the collapse pits is mostly less than 1 000 m^2, the average area is 918.98 m^2, and the depth is generally less than 10 m. Some collapse pits have a depth greater than 20 m and area greater than 5000 m^2.

In more than 80% of the karst collapse areas in Wuhan City, the upper cover layer is a Quaternary loose alluvial with a fluvial binary structure: the upper part is clay, and the lower part is sandy soil. **Figure 1** shows the recent ground collapse statistics for Wuhan.

ESTABLISHMENT OF A 3D GEOLOGICAL STRUCTURE MODEL OF THE SURVEY AREA

According to statistics, most of the karst collapses in Wuhan are currently distributed in the Baishazhou karst belt, which is located at the core of the Xinlong-Leopardsui complex inverted syncline. In this study, the two sides of the Yangtze River along the Baishazhou karst belt in the central and southern urban areas of Wuhan City were selected as the key survey areas, with a total area of 123.68 km^2, involving three central urban areas of the city, including Wuchang District, Hanyang District, and Hongshan District, and the Wuhan Economic and Technological Development Zone. The area ranges from east to west of the South Lake in Hongshan District, west to Longyang Village in Hanyang District, north to Wuhan Yangtze River Bridge, and south to Zhuankou to Qingling District.

Most of the bedrock in the study area is hidden under the Quaternary soil layer, and the main lithology is limestone, marl, mudstone, dolomite, and quartz sandstone. The Quaternary loose accumulation layers are mainly alluvial, flood alluvial, lacustrine, and artificial fills induced by human engineering activities. The Quaternary soil layer has a thickness in the range of 10–50 m and composed of silty clay, sand, and gravel. The types of groundwater in the area include loose rock pore water, clastic rock fissure water, and carbonate rock fissure karst water. Underground engineering construction in such a geological body can cause adverse geological disasters such as ground subsidence, piping, and ground collapse. A 3D geological model is a mathematical modeling process based on multisource geological data, such as geological borehole stratification, profile, fractures, and folds, combined with certain mathematical simulation methods. This study used a 3D modeling technology to establish a 3D geological structure model of the survey area, combined with existing geological data, and analyzed the causes of ground collapse disasters in the area.

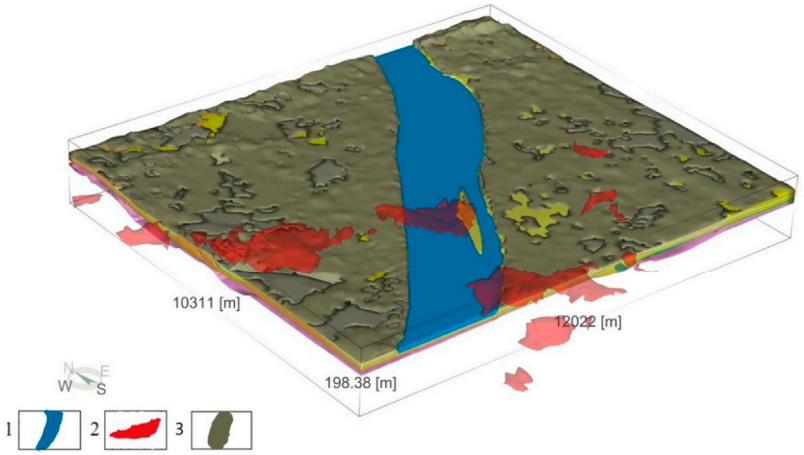

1. Yangtze River; 2. Carbonate rock; 3. Quaternary strata

FIGURE 2 | Diagram of karst distribution. 1. Yangtze River; 2. Carbonate rock; 3. Quaternary strata.

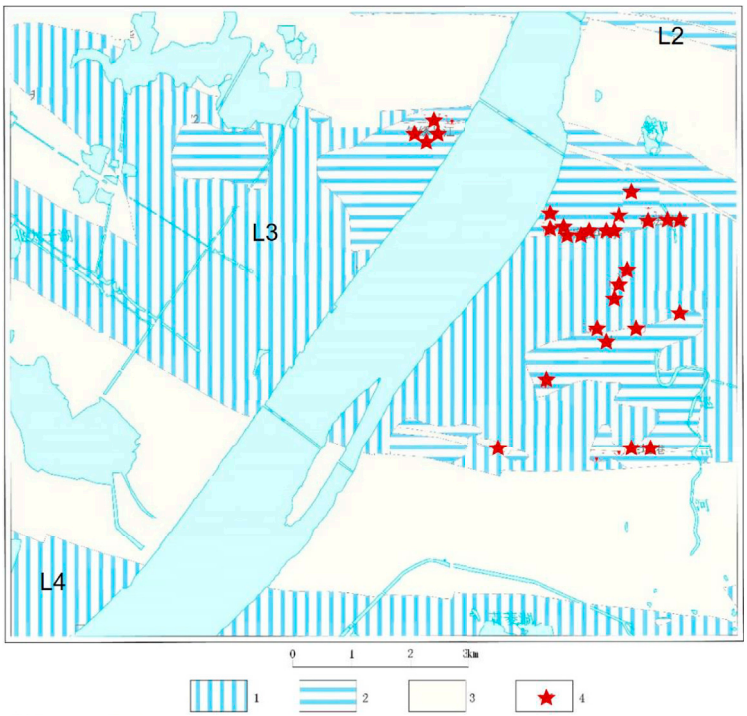

1. Buried karst area; 2. Covered karst area; 3. Nonsoluble rock area; 4. Karst collapse

FIGURE 3 | Distribution of karst ground collapse in the study area. 1. Buried karst area; 2. Covered karst area; 3. Nonsoluble rock area; 4. Karst collapse.

In this study, data from 4416 boreholes were collected, from which 2433 bedrock holes were selected as effective holes for modeling. Based on the regional survey data, the standard layered table of drilling holes in the study area was summarized, and the effective holes were sorted out and analyzed based on the layered table. Subsequently, depending on the requirements of the basic data of modeling, a preliminary model was built, and the fine processing work was conducted according to the geological section and geophysical profile. The final modeling work was completed. The area of the constructed 3D model was 123.68 km^2. **Figures 2**, **3** show the final karst distribution

diagram and the distribution map of the karst ground collapse in the study area, respectively.

From **Figures 2**, **3**, three hidden soluble rock belts can be seen in the study area. The distribution area of the hidden soluble rock was 71.43 km^2, accounting for 57.75% of the total area of the study area, including covered karst area and buried karst area. Covered karst area refers to the area where carbonate rock is mostly covered by Quaternary sediments, and only sporadic bedrock outcrops can be seen locally. Buried karst area refers to the area where Cretaceous-Paleogene mudstone and siltstone cover directly above the carbonate rock. Because of the thick cover, karst phenomenon is not exposed on the surface. The concealed soluble rock in the area are generally distributed in the NWW-SEE direction. In some areas, the karst belts are bent or discontinuous due to the influence of the structure, and the belt width is in the range of 0.8–6 km. Controlled by the structure and topography, the concealed soluble rock is mainly located in the core of the syncline, and a few in the wing of the syncline. The soluble rock strata is mainly limestone of the Lower Triassic Daye Formation (T_1d), limestone of the Middle Permian Qixia Formation (P_2q), and dolomitic limestone of the Upper Carboniferous Huanglong-Dapu Formation (C_2h + d). The study area can be roughly divided into three concealed soluble rock belts from north to south.

(1) Bridge Karst Belt (L2): The concealed karst area is located in the southern end of the bridge karst belt, Canghu Road in Hanyang District-Yangtze River coast-Wuchang District Zhongtie Building area. The distribution area is about 1.21 km^2, accounting for 1.69% of the total area of the soluble rock belt in the study area. The first-order cover layer is an alluvial layer with a dual structure, and the higher order is the old clay. The area is covered karst area, and karst collapse occurred at the Civil Affairs School in Wuchang District outside the northern research area.

(2) Baishazhou Karst Belt (L3): The hidden karst area is located in the middle of the Baishazhou karst belt along the Yangtze River, Taizi Lake-Hanyang National Expo Center-Zhangjiawan-Xunsi River area, located in the Xinlong-Leopard-Zui complex. The total area of the belt is 60.26 km^2, accounting for 84.36% of the total area of the soluble rock belt in the study area, with a north-south width in the range of 2.45–6 km. First-order terrace capping sand layer is developed and in direct contact with the limestone. Most of the belts are buried karst areas, and only areas along the Yangtze River in the north and the Xunsi River in the southeast are mainly covered karst areas. This area has seen 78% of the karst collapses that occurred in Wuhan, and the collapses are mainly distributed in Baishazhou Avenue, Qingling Township, Wutai Gate, Zhangjiawan and other locations along the Yangtze River.

(3) Zhuankou Karst Belt (L4): This hidden karst area is located in the area of Jiangyongdi-Qinglingsi-Xingang Village at the northern end of the Zhuankou karst belt. The distribution area of this belt is about 9.96 km^2, accounting for 13.9% of the total area of the soluble rock belt in the study area, and the caprock is old clay. The karst belt along the Yangtze River is mainly a buried karst area.

TEMPORAL AND SPATIAL DISTRIBUTION CHARACTERISTICS OF KARST GROUND SUBSIDENCE IN STUDY AREA

Temporal Distribution

Temporal, karst ground collapse accidents in the study area have mainly occurred after 2005. In recent years, the frequency has increased, the time interval has decreased, and such accidents may recur after a period of time. **Figure 4** shows the time distribution of the karst collapse in the study area. Since 2009, karst ground collapse accidents have occurred almost every year, including 5 in 2009 and 4 in 2014. This is related to the increase in urban development and engineering construction activities in this area in recent years. Since the Wuhan government attaches great importance to the prevention and control of karst collapse, and strengthens the engineering control in karst areas, the frequency of karst collapse accidents decreases after 2015. Temporally, such incidents appear every month; however, they are particularly serious in the April-August period, which is the rainy season in Wuhan City. The rainfall is abundant, the groundwater level fluctuates significantly, and the infiltration of rainwater changes the physical and mechanical properties of the overlying soil and becomes the driving force for ground collapse in hidden karst areas.

Spatial Distribution

Judging from the geological environment of the collapse point, all karst ground collapses in the region are distributed in the binary structure alluvium (Qh) of the first terrace of the Yangtze River, the Baishazhou karst belt, and the Xinlong-Leopardsui complex inverted syncline. In the core, the karst confined water head in the collapsed section is lower than the alluvial pore confined water head. The overlying alluvial of the karst ground collapse in the area is the Quaternary loose alluvial with a binary structure composed of upper clay and lower sand in the first-order terrace of the Yangtze River. The alluvial thickness is mostly between 20 m and 35 m. Most of the underlying rock is the lower Triassic Daye Formation limestone (T_1d) and the Permian Middle Qixia Formation limestone (P_2q). There are some developed karst fissures and karst caves with a height range of 0.1–5 m. Although there is carbonate rock karst bands in the old clay of the second and third terraces of the Yangtze River, there has never been a ground collapse accident because of the lack of soil caves.

TYPICAL CASE ANALYSIS

The karst subsidence area of Fenghuo Village is located on the east side of the study area, around Fenghuo Village, Qingling Street, Hongshan District, Wuhan City. It is located at the front edge of the first-level terrace of the Yangtze River, covering an area of 0.12 km^2. There have been three karst collapses in the area: the karst collapse of Qiaomuwan in Fenghuo Village in 2000; the karst collapse of the Jiangnan Zhumu Market in Fenghuo Village in 2005; and the karst collapse of the steel market in Fenghuo Village in 2009. The karst collapse of Qiaomuwan in Fenghuo Village in 2000 is selected as a typical case for analysis.

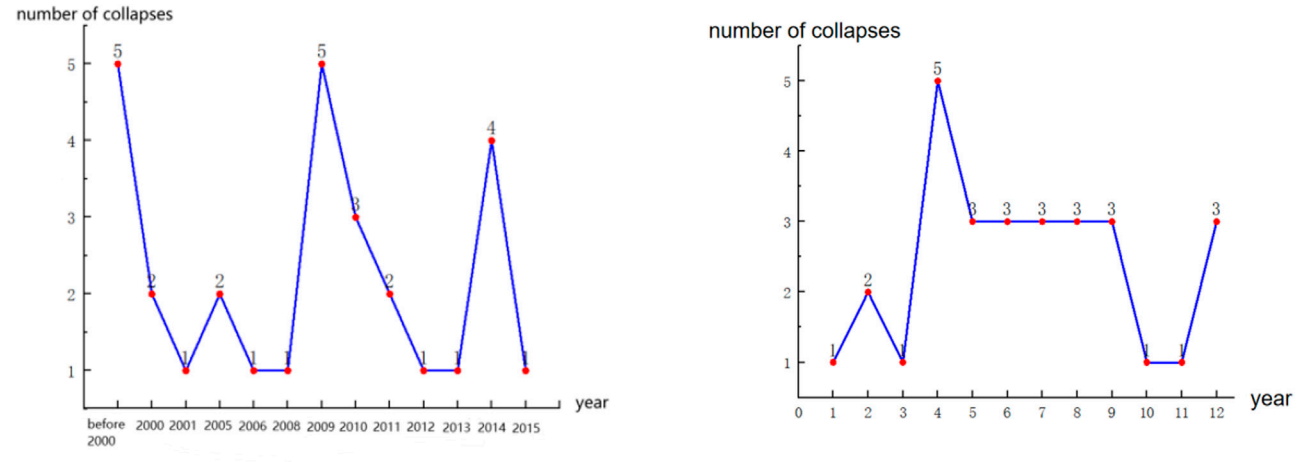

FIGURE 4 | Temporal distribution of karst collapse in the study area

FIGURE 5 | Karst collapse incidents in Fenghuo Village. Karst collapse in Fenghuo Village (2000), Karst collapse in Fenghuo Village (2009).

As shown in **Figure 5**, on 6 April 2000, the largest karst collapse in the history of Wuhan City occurred in Qiaomuwan of Fenghuo Village. There were 19 collapse pits, which were concentrated in the second and third groups of the residential areas and vegetable fields. Among them, the plane shape of the largest collapse pit is oval, with a long axis of 54 m, a short axis of 33 m, and a depth of 7.8 m. The plane shape of the smallest pit is circular, with a diameter of 2.0 m and a depth of 2.0 m. In August 2005, another ground subsidence occurred near the original subsidence pit. The subsidence pit is oval in the plan and dish-shaped at the section, with a long axis of 4.5 m, a short axis of 4.0 m, and a visible depth of 1.07 m.

This area belongs to the front of the first terrace of the Yangtze River in terms of topography and landform, where is an alluvial plain landform, and aquifer thickness is 15.00–16.19 m, permeability coefficient is 29.32–37.80 m/d. In terms of the geological structure, it is located in the core of the Heyeshan synclin, which is a multilayer structure. The underlying bedrock is the lower Triassic Daye Formation (T_1d) limestone. **Figures 6**, **7** show the geological profile and the 3D morphological schematic of the karst distribution, respectively. The karst collapse area of Fenghuo Village has karst caves in the limestone. The overlying soil layer is relatively loose, with sandy soil in the middle. The karst development volume is large, and the overlying soil layer is thin. The surface karst zone is located in the shallow part of the soluble rock, mostly in the range of 5 m of the bedrock surface, and the buried depth is 27–36 m. It is connected with the lower karst development area by the fracture channel and has hydraulic interaction.

Analysis of Karst Collapse Evolution Process

The karst ground collapse process of Qiaomuwan in Fenghuo Village can be characterized by soil cave formation, development and final ground collapse. The evolution process of the karst

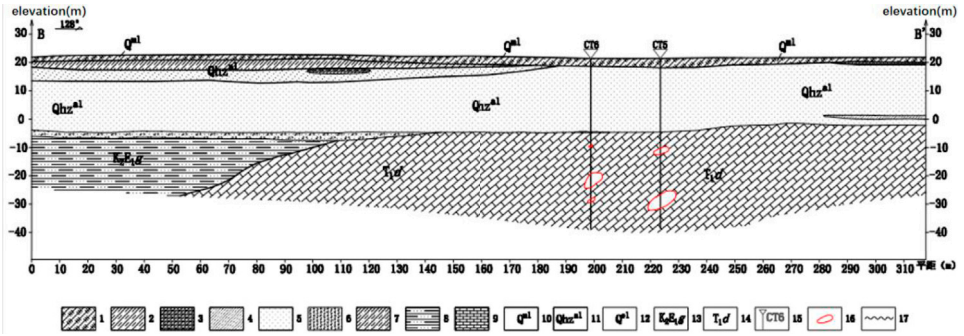

1. Miscellaneous fill; 2. Silty clay; 3. Muddy-silty clay; 4. Silty soil; 5. Fine sand; 6. Medium and coarse sand with gravel; 7. Residual soil; 8. Silty siltstone; 9. Limestone; 10. Quaternary artificial fill; 11. Quaternary alluvial layer; 12. Quaternary residual layer; 13. Cretaceous-Paleogene Gonganzhai Formation; 14. Lower Triassic Daye Formation; 15. Drilling number; 16. Cave; 17. Unconformity boundary.

FIGURE 6 | Geological profile of Qiaomuwan collapse area in Fenghuo Village. 1. Miscellaneous fill; 2. Silty clay; 3. Muddy-silty clay; 4. Silty soil; 5. Fine sand; 6. Medium and coarse sand with gravel; 7. Residual soil; 8. Silty siltstone; 9. Limestone; 10. Quaternary artificial fill; 11. Quaternary alluvial layer; 12. Quaternary residual layer; 13. Cretaceous-Paleogene Gonganzhai Formation; 14. Lower Triassic Daye Formation; 15. Drilling number; 16. Cave; 17. Unconformity boundary.

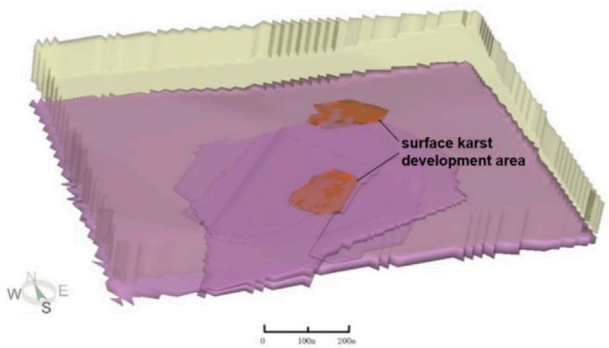

FIGURE 7 | 3D shape of karst distribution in Qiaomuwan karst collapse area of Fenghuo Village.

ground collapse can be roughly divided into three stages; **Figure 8** shows the evolution process diagram.

1) Primitive stability stage: There is a certain head difference between Quaternary pore water and karst water. Quaternary pore water supplies karst water; however, the seepage gradient is small, and the sand layer is in a relatively stable state.
2) The combined action stage of artificial and natural factors: In this stage, groundwater is artificially extracted, and karst water is strongly exploited to form a drop funnel, resulting in the seepage of pore water to promote the loss of small particles in the loose deposits, and a small soil cave is formed near the karst gap. Under the effect of seepage force of rainfall, noncohesive particles (such as sand particles) are rapidly lost, and the soil cave expands.
3) Collapse stage: After the soil cave reaches a certain scale, the upper cover layer is close to the critical arch height. Under the action of triggering factors such as ground vehicle load, the collapse-inducing force of the soil arch becomes greater than the anti-slump force, the soil arch is damaged, and the soil at the top of the cave loses its balance. This causes a rapid slump, affecting the ground and eventually forming a ground collapse.

Mechanism Analysis of Karst Collapse

The factors leading to karst ground collapse are divided into internal and external factors. Internal factors are related to the geological environment of the region, and external factors are related to dynamic conditions.

The karst geological structure of the Qiaomuwan karst collapse in Fenghuo Village is a three-layer structure: cohesive soil in the upper part, sandy soil in the middle, and soluble rock in the lower part. Under the effect of external factors, this geological structure is directly formed; or when the cohesive soil on the soluble rock is damaged, the sand particles leak out, and the ground collapses. The karst collapse area of Fenghuo Village has two types of groundwater: Quaternary pore-confined water in the upper silty sand layer and fractured karst water in the underlying carbonate rock. The three periods of karst ground collapse were all in the dry season of Wuhan City, with less rainfall, and the water level of the Yangtze River remained low. Before the collapse, there were pumping wells operating in the area. According to the data, the pore confined water was exploited. When the exploitation rate was 70 m^3/h, the drawdown could reach 9.90 m. According to Kusakkin formula, the influence radius of arbor bay in Fenghuo village can be obtained when mining pore confined water.

$$R = 2S\sqrt{HK} \tag{1}$$

where, R is radius of influence (m); S is drawdown (m); H is aquifer thickness (m); K is permeability coefficient (m/d).

According to **Eq. 1** and previous drilling data, taking aquifer thickness of 15 m, permeability coefficient of 30 m/d, the influence radius was about 420 m. In the karst collapse area of Fenghuo Village, under natural conditions, the pore water level was higher

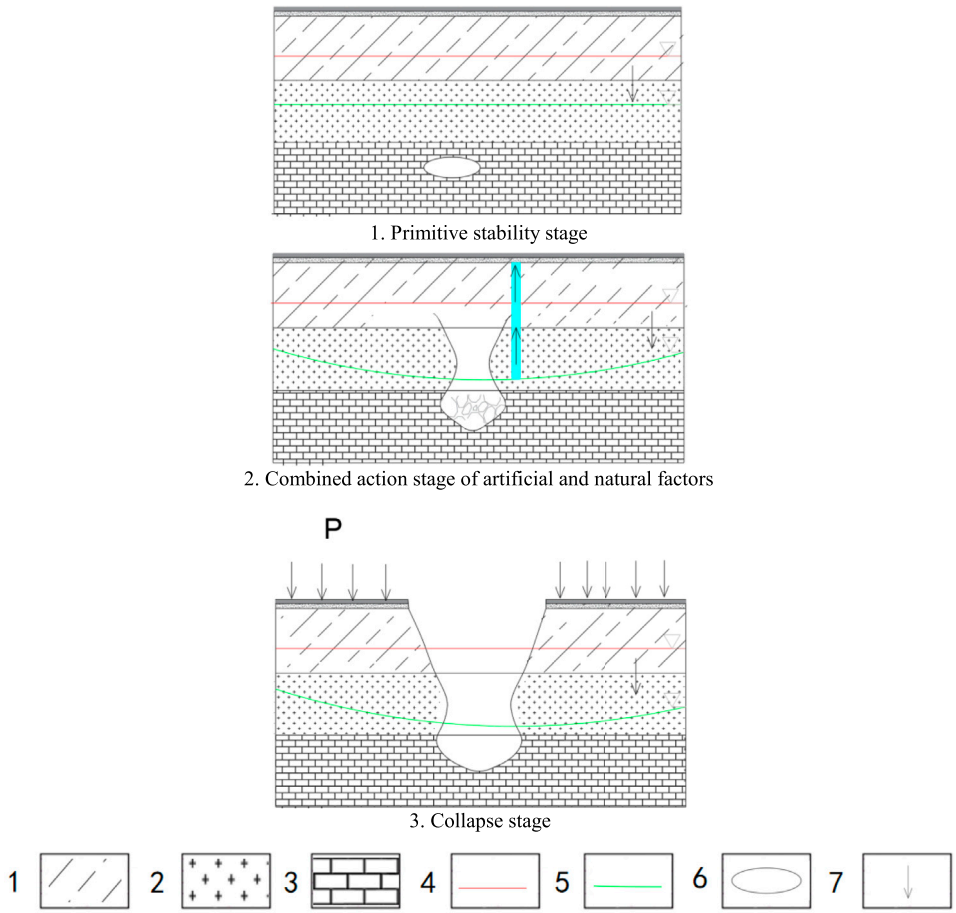

FIGURE 8 | Schematic of the evolution process of karst collapse in Fenghuo Village. 1. Primitive stability stage, 2. Combined action stage of artificial and natural factors, 3. Collapse stage. 1. Viscous soil 2 Sandy soil 3 Soluble rock 4 Pore water level 5 Karst water level 6 Cavity 7 Flow direction.

than the karst water level, and the pore water moved vertically downward to replenish the karst water. Owing to its permeability, the water carried the overlying sand particles into the lower karst pipeline system. When the pumping wells were continuously pumped with a high intensity (such as the drought resistance in the dry season), the water level dropped sharply to form a landing funnel. The radius of the landing funnel was greater than 420 m, the central water level drop was greater than 9.90 m, and the edge and central hydraulic gradient of the landing funnel was greater than 23.57‰. When the pore water level dropped below the karst water level, the karst water recharged the pore water from the bottom to the top, and the water moved upward. The uplift pressure of the karst water also led to soil destruction. The seepage force of the water and the uplift pressure of the water showed alternate characteristics, resulting in a potential erosion of the fine particles and the formation of disturbed soil layers (soil holes) in the soil. With the continuous development of the soil hole, a large-scale collapse occurred.

The causal mechanism of the collapse is mainly the effect of subsurface erosion and seepage caused by the exploitation of groundwater. It is a type of collapse largely influenced by human factors.

CONCLUSION

The geological environment of Wuhan city is complex. Carbonate rocks is widely distributed and covered by Quaternary strata. Due to the solubility and water insulation of rocks, they could be divided into six karst belts. The existence of karst voids in the karst belt, and the combination of Quaternary loose alluvial deposits and underlying limestone strata with a binary structure composed of sand in the lower part and clay in the upper part formed the geological basis for the occurrence of karst ground collapse disasters. Taking the two sides of the Yangtze River in the Baishazhou karst belt in the central and southern parts of Wuhan city as the key research area, a 3D geological modeling was conducted using data collected from the boreholes, and the karst belt in the study area was displayed using a visual 3D model. The karst belt was composed of some carbonate rocks with large volume and certain connections, which were close to each other. The karst ground collapse disaster points in the study area were

distributed in the Baishazhou karst belt. The geological environment of the collapse points was roughly the same, i.e., the combination of Quaternary sand and cohesive soil and underlying limestone.

The Fenghuo Village was selected as a typical karst ground subsidence area for the research. From the geological section and 3D geological model, karst cavities were found in the limestone of this village, and the Quaternary soil layer was an artificial filling soil layer, which was relatively loose. Under normal conditions, the karst water level in the region was lower than the pore water level, and the pore water supplied karst water downward, which was in a stable state. The area is filled with engineering activities. Karst water had been extracted for engineering construction, and the water level dropped. At this time, the karst cavity continued to expand under the effect of permeability until the coating soil layer on the top of the cave reached its critical height. Under the action of traffic load acting on the road, the collapse force of the soil arch was greater than the anti-collapse force, and the soil arch was destroyed, ultimately leading to collapse.

DATA AVAILABILITY STATEMENT

The raw data supporting the conclusions of this article will be made available by the authors, without undue reservation.

AUTHOR CONTRIBUTIONS

QH: data curation, writing—original draft preparation. FT: conceptualization, supervision, writing—reviewing and editing. ZP: conceptualization, methodology. LT: resources. YJ: investigation, funding acquisition. SL: resources. HP: resources.

FUNDING

This work was supported by the National Natural Science Foundation of China (Grant nos. 51879245 and 41920104007), and the Fundamental Research Funds for the Central Universities, China University of Geosciences (Wuhan) (No. CUGCJ1821).

REFERENCES

Atzori, S., Baer, G., Antonioli, A., and Salvi, S. (2015). InSAR-based Modeling and Analysis of Sinkholes along the Dead Sea Coastline. *Geophys. Res. Lett.* 42 (20), 8383–8390. doi:10.1002/2015GL066053

Feng, Z. H., Li, X. F., Zhang, M. H., and Liang, J. C. (2001). Distribution of Karst Collapse and its Relation to Geological Structures in the Guilin Urban and Suburban Areas, Guangxi Province. *J. Geol. Hazards Environ. Preserv.* 12 (2), 16–20. (in Chinese).

Gutiérrez, F., Parise, M., De Waele, J., and Jourde, H. (2014). A Review on Natural and Human-Induced Geohazards and Impacts in Karst. *Earth-Science Rev.* 138, 61–88. doi:10.1016/j.earscirev.2014.08.002

Hassen, I., Gibson, H., Hamzaoui-Azaza, F., Negro, F., Rachid, K., and Bouhlila, R. (2016). 3D Geological Modeling of the Kasserine Aquifer System, Central Tunisia: New Insights into Aquifer-Geometry and Interconnections for a Better Assessment of Groundwater Resources. *J. Hydrology* 539, 223–236. doi:10.1016/j.jhydrol.2016.05.034

He, X., Koch, J., Sonnenborg, T. O., Jørgensen, F., Schamper, C., and Refsgaard, J. C. (2014). Transition Probability-Based Stochastic Geological Modeling Using Airborne Geophysical Data and Borehole Data. *Water Resour. Res.* 50 (4), 3147–3169. doi:10.1002/2013WR014593

Keqiang, H., Bin, W., and Dunyun, Z. (2004). Mechanism and Mechanical Model of Karst Collapse in an Over-pumping Area. *Env. Geol.* 46 (8), 1102–1107. doi:10.1007/s00254-004-1099-8

Kessler, H., Mathers, S., and Sobisch, H.-G. (2009). The Capture and Dissemination of Integrated 3D Geospatial Knowledge at the British Geological Survey Using GSI3D Software and Methodology. *Comput. Geosciences* 35 (6), 1311–1321. doi:10.1016/j.cageo.2008.04.005

Klimchouk, A., and Andrejchuk, V. (2005). Karst Breakdown Mechanisms from Observations in the Gypsum Caves of the Western Ukraine: Implications for Subsidence Hazard Assessment. *Environ. Geol.* 48 (3), 336–359. doi:10.1007/s00254-005-1279-1

Koutepov, V. M., Mironov, O. K., and Tolmachev, V. V. (2008). Assessment of Suffosion-Related Hazards in Karst Areas Using GIS Technology. *Environ. Geol.* 54 (5), 957–962. doi:10.1007/s00254-007-0888-2

Li, Z. G., Xiao, S. D., Pan, Y. H., and Lu, S. W. (2013). The Hazard Assessment of Karst Surface Collapse Risk Zoning Based on BP Neural Network in Wuhan City. *Appl. Mech. Mater.* 405-408, 2376–2379. doi:10.4028/www.scientific.net/amm.405-408.2376

Luo, X. J. (2014). Division of "Six Belts and Five Types" of Carbonate Region and Control of Karst Geological Disaster in Wuhan. *J. Hydraulic Eng.* 45 (02), 171–179. (in Chinese). doi:10.13243/j.cnki.slxb.2014.02.006

Shalev, E., and Lyakhovsky, V. (2012). Viscoelastic Damage Modeling of Sinkhole Formation. *J. Struct. Geol.* 42, 163–170. doi:10.1016/j.jsg.2012.05.010

Thierry, P., Prunier-Leparmentier, A.-M., Lembezat, C., Vanoudheusden, E., and Vernoux, J.-F. (2009). 3D Geological Modelling at Urban Scale and Mapping of Ground Movement Susceptibility from Gypsum Dissolution: The Paris Example (France). *Eng. Geol.* 105 (1-2), 51–64. doi:10.1016/j.enggeo.2008.12.010

Vollgger, S. A., Cruden, A. R., Ailleres, L., and Cowan, E. J. (2015). Regional Dome Evolution and its Control on Ore-Grade Distribution: Insights from 3D Implicit Modelling of the Navachab Gold Deposit, Namibia. *Ore Geol. Rev.* 69, 268–284. doi:10.1016/j.oregeorev.2015.02.020

Yilmaz, I., Marschalko, M., and Bednarik, M. (2011). Gypsum Collapse Hazards and Importance of Hazard Mapping. *Carbonates Evaporites* 26 (2), 193–209. doi:10.1007/s13146-011-0055-4

Zhu, L.-f., Li, M.-j., Li, C.-l., Shang, J.-g., Chen, G.-l., Zhang, B., et al. (2013). Coupled Modeling between Geological Structure Fields and Property Parameter Fields in 3D Engineering Geological Space. *Eng. Geol.* 167, 105–116. doi:10.1016/j.enggeo.2013.10.016

Zuo, J.-P., Peng, S.-P., Li, Y.-J., Chen, Z.-H., and Xie, H.-P. (2009). Investigation of Karst Collapse Based on 3-D Seismic Technique and DDA Method at Xieqiao Coal Mine, China. *Int. J. Coal Geol.* 78 (4), 276–287. doi:10.1016/j.coal.2009.02.003

Conflict of Interest: The authors declare that the research was conducted in the absence of any commercial or financial relationships that could be construed as a potential conflict of interest.

Publisher's Note: All claims expressed in this article are solely those of the authors and do not necessarily represent those of their affiliated organizations, or those of the publisher, the editors and the reviewers. Any product that may be evaluated in this article, or claim that may be made by its manufacturer, is not guaranteed or endorsed by the publisher.